Influence of coarse aggregate settlement induced by vibration on long-term chloride transport in concrete

a numerical study

Cai, Yuxin; Liu, Qing feng; Meng, Zhaozheng; Chen, Mengzhu; Li, Weihua; Šavija, Branko

DOI
10.1617/s11527-022-02038-z

Publication date
2022

Document Version
Final published version

Published in
Materials and Structures/Materiaux et Constructions

Citation (APA)
Cai, Y., Liu, Q. F., Meng, Z., Chen, M., Li, W., & Šavija, B. (2022). Influence of coarse aggregate settlement induced by vibration on long-term chloride transport in concrete: a numerical study. *Materials and Structures/Materiaux et Constructions*, *55*(9), Article 235. https://doi.org/10.1617/s11527-022-02038-z

Materials and Structures (2022)55:235
https://doi.org/10.1617/s11527-022-02038-z

ORIGINAL ARTICLE

Influence of coarse aggregate settlement induced by vibration on long-term chloride transport in concrete: a numerical study

Yuxin Cai · Qing-feng Liu · Zhaozheng Meng · Mengzhu Chen · Weihua Li · Branko Šavija

Received: 1 June 2022 / Accepted: 24 August 2022

Abstract High-frequency vibration helps to improve the compactness of concrete, but also causes the settlement of coarse aggregates (CAs) and then affects the durability of hardened concrete. In this paper, a numerical study combining multi-phase CA settlement model and multi-component ionic transport model is performed to understand the influence of vibration-induced settlement on long-term chloride transport in concrete. Through parametric analysis, the influence mechanism of relevant factors on both chloride profile distribution and reinforcement corrosion initiation is discussed in detail. The results indicate that with the increase of vibration time, a decrease of chloride concentration appears in the bottom part of concrete specimen and a significant increase in the top part, because more CAs deposit in the bottom layer. Due to sedimentation, a more obvious fluctuation of chloride concentration along the height direction can be observed in the concrete mixed with a larger density and particle size of CAs. According to the model prediction, the corrosion of the top steel bar initiates 1.03–1.80 years earlier than that of the bottom steel bar under the same parameters. In practical engineering, special attention should be paid on the stability of fresh concrete and vibrating procedures to avoid obvious CA settlement.

Keywords CA settlement · Vibration · Chloride transport · Corrosion initiation · Durability · Numerical model

Y. Cai · Q. Liu (✉) · Z. Meng
State Key Laboratory of Ocean Engineering, School of Naval Architecture, Ocean and Civil Engineering, Shanghai Jiao Tong University, Shanghai 200240, China
e-mail: liuqf@sjtu.edu.cn

Y. Cai · Q. Liu · Z. Meng
Shanghai Key Laboratory for Digital Maintenance of Buildings and Infrastructure, Shanghai 200240, China

M. Chen · W. Li
School of Chemical Engineering and Technology, Sun Yat-sen University, Zhuhai 519082, China

B. Šavija
Microlab, Faculty of Civil Engineering and Geosciences, Delft University of Technology, 2628 CN Delft, the Netherlands

Published online: 07 November 2022

1 Introduction

Large-sized modern buildings with complex geometry and dense reinforcement arrangement usually require fresh concrete to have enough flowability to be poured easily and sufficient stability to ensure the quality of reinforced concrete structures. However, while many studies focus on the flowability of concrete mixtures [1–4], there are limited studies correlating vibration-induced stability issue with long-term performance of hardened concrete. Stability refers to the ability of fresh concrete to maintain a uniform distribution of various components of mixtures during the casting and

vibrating consolidation process [5]. Whether in the laboratory or on site, concrete mixtures usually need high-frequency vibration to achieve a dense state. However, vibration also leads to the settlement of coarse aggregates (CAs), which makes the fresh concrete exhibit a poor stability [6, 7].

After concrete hardening, the CA settlement has an adverse impact on the mechanical strength and durability of reinforced concrete. Khayat et al. [8] pointed out that settlement and segregation might produce local defects, leading to variations in the design strength of hardened concrete and the bond behaviour between steel reinforcement and concrete at different heights. Megid and Khayat [9] found that, due to the CA sedimentation of fresh concrete, a porous cement mortar layer with poor appearance quality was formed on the top surface of concrete specimens, where was vulnerable to cracking and facilitating the ingress of harmful substances. The experimental results of Gao et al. [10] indicated that both mechanical strength and chloride permeability variations along the height direction increased linearly with the degree of CA settlement, and the maximum difference rates of the two could reach 12.4% and 72.1%, respectively. Panesar and Shindman [11] also reported that the transport properties varied along the casting direction, and the durability performance was worse for the top surface of concrete specimens in comparison to the bottom surface. In authors' prior studies [12, 13], it was found that due to the occurrence of CA settlement, when the height position of concrete core samples increased from 150 to 750 mm, the chloride permeability increased by 50%, resulting in earlier corrosion initiation of steel bars arranged at a higher position.

Chloride-induced corrosion of steel bars plays a crucial role in affecting the durability of reinforced concrete [14–20]. Under the effects of diffusion, electrochemical migration, convection and capillary adsorption, chloride ions from the environment reach the surface of embedded steel bars through the concrete cover. Afterwards, a series of complex chemical reactions between chloride ions and the surface of steel bars lead to a local damage of passive film, and then reinforcement corrosion begins to occur through a depassivation process [21–25]. Therefore, it can be considered that the quality of concrete cover plays a critical role in the protection of steel bars. It is worth noting that in some large-sized marine-exposed structures, such as offshore concrete and bridge piers, the settlement phenomenon is more obvious, and it easily results in the serious heterogeneous distribution of CAs. Under the action of gravity, more CAs settle to the bottom part of structural concrete, which will increase the tortuosity of chloride transport path after concrete hardening. On the contrary, the ability of concrete cover to resist chloride penetration becomes weaker in the top part because more porous cement mortars exist in this area.

Note that due to the opacity of concrete, it seems impossible to observe the CA settlement directly with naked eye. Hence, some indirect experimental methods and techniques are used to assess the heterogeneity of CA distribution, such as radioactive element labelling [26], image processing [27], electrical conductivity [28], ultrasonic velocity [29] and gamma-ray attenuation [30]. However, it can be seen that these methods and techniques are mainly based on the experimental observations. In order to visualize and parameterize the information of every CA particle at any vibration time and any location, a 3-D model for CA settlement has been developed in previous study [31]. Considering that experimental investigations are time-consuming and expensive, particularly for the long-term deterioration of reinforced concrete, it is necessary to propose a cost-effective numerical method to link such a rheological problem with the durability of concrete, thereby revealing the influence mechanism of CA settlement on chloride transport.

Therefore, the main objective of this paper is to adopt the settlement model to provide input for the ionic transport model to study the influence of vibration-induced CA settlement on long-term chloride ingress in hardened concrete. Parametric studies of influencing factors such as the vibration time, the density and particle size of CAs, and the diffusivity property of interfacial transition zones (ITZs) on chloride concentration distribution along the height direction are performed and discussed, and the impact of these factors on the initiation time of reinforcement

corrosion is predicted. The findings of this study can provide a deeper understanding of such a noteworthy durability issue caused by CA settlement.

2 Numerical implementation

2.1 CA settlement induced by vibration

The modelling approach for simulating CA settlement has been previously verified and published [31], and is briefly introduced here for the completeness and logicality of the article framework. The interested readers can refer to the original study for more details.

In vibrated concrete mixtures, a single CA particle is mainly affected by gravity, buoyancy and viscous resistance [32–34], as displayed in Fig. 1.

The expressions of gravity (G) and buoyancy (B) are shown in Eqs. (1) and (2), respectively.

$$G = \rho_a V g = \frac{1}{6}\pi\rho_a d^3 g \tag{1}$$

$$B = \rho_m V g = \frac{1}{6}\pi\rho_m d^3 g \tag{2}$$

where ρ_a and ρ_m represent the CA density and mortar density, respectively, d is the CA particle size, and g is the gravitational acceleration.

In general, when Reynolds number is below 2100, the flow is considered to be laminar flow. When it is higher than 4000 (or 10,000 in some studies), the flow

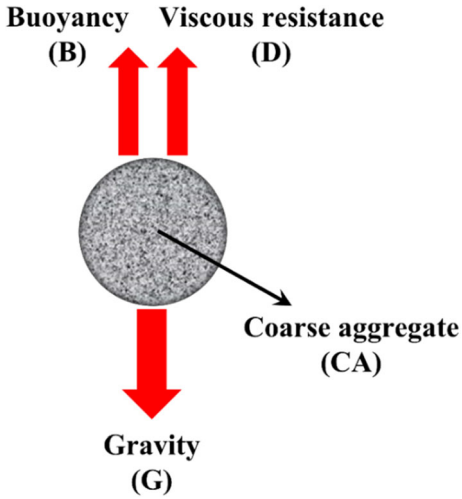

Fig. 1 Force analysis of a single CA in vibrated concrete mixtures (adapted from [31])

is turbulent flow. Since the movement velocity of CAs in concrete mixtures is rather slow, Reynolds number is much less than 2100 and the flow type around the CA particles is considered to be laminar. Based on Stokes law, the viscous resistance (D) can be expressed as:

$$D = 3\pi v d \eta_{pl} \tag{3}$$

where v is the movement velocity of CAs, and η_{pl} is the plastic viscosity of mortars.

Assuming that the density and plastic viscosity of mortars remain constant during the vibration, the CA particle will eventually settle at a constant rate as D increases to a value that can counteract the resultant force of G and B. At this time, the final settlement velocity (v_s) can be derived as Eq. (4).

$$v_s = \frac{d^2 g(\rho_a - \rho_m)}{18\eta_{pl}} \tag{4}$$

Through integral calculation, the equation describing the relationship between the CA settlement height (Δh) and vibration time (t) can be obtained, as show in Eq. (5). Appendix 1 gives the specific solution process of Eq. (5).

$$\Delta h = \frac{d^2 g(\rho_a - \rho_m)}{18\eta_{pl}} \cdot \left\{ t - \frac{d^2\rho_a}{18\eta_{pl}} \cdot \left[1 - \exp\left(-\frac{18\eta_{pl}}{d^2\rho_a} \cdot t \right) \right] \right\} \tag{5}$$

Because the CA particle size is usually on the scale of 10^{-3} m, the value of constant and exponential terms ($\frac{d^2\rho_a}{18\eta_{pl}} \cdot \left[1 - \exp\left(-\frac{18\eta_{pl}}{d^2\rho_a} \cdot t \right) \right]$) in Eq. (5) is much smaller than that of the linear term (t). Thus, the settlement height is further expressed by Eq. (6).

$$\Delta h = \frac{d^2 g(\rho_a - \rho_m)}{18\eta_{pl}} \cdot t \tag{6}$$

However, each CA particle will also be affected by the interaction with other particles in vibrated concrete. Under this circumstance, η_{pl} in Eq. (6) can be approximately replaced by the plastic viscosity of concrete mixtures (η_{pl}'), so as to consider the interaction between CAs [35–37]. Moreover, the test value of η_{pl}' needs to be calibrated, since fresh concrete no longer completely follows a Bingham model when exposed to external vibration. Hence, the actual CA settlement height (Δh') can be modified as:

$$\Delta h' = \frac{d^2 g(\rho_a - \rho_m)}{18k\eta'_{pl}} \cdot t \tag{7}$$

where k is the non-dimensional calibration coefficient for η_{pl}', which is determined in [31].

2.2 Chloride transport in concrete

Diffusion, as the dominant driving force, describes the transport process of ionic species in saturated concrete. Generally, the process of chloride transport can be articulated by Fick's second law, as show in Eq. (8).

$$\frac{\partial C}{\partial t} = D_{Cl}\frac{\partial^2 C}{\partial x^2} \tag{8}$$

where C is the chloride concentration, t is the diffusion time, D_{Cl} is the diffusion coefficient of chloride ions, and x is the diffusion depth.

However, Fick's law only expresses the primary form of ionic transport. In order to comprehensively understand and estimate the chloride transport behaviour in concrete, the influence of the porosity of concrete, chloride binding effect and electrochemical coupling between multi-species needs to be taken into consideration.

2.2.1 Porosity

The chloride diffusion rate is directly related to the porosity of concrete [38]. According to [39], an empirical equation, as shown in Eq. (9), can be used to estimate the porosity of cement mortars (φ).

$$\varphi = \frac{w/c - 0.17 \times \omega}{w/c + 0.32} \tag{9}$$

Here, ω refers to the hydration degree. Regarding the determination of hydration degree value, Bentz et al. [40] established an additional equation providing a relationship between ω and water to cement ratio (w/c):

$$\omega = 1 - \exp(-3.15 \times w/c) \tag{10}$$

At present, some well-developed theoretical or empirical formulas are usually used to assess the chloride diffusion coefficient [41]. In this study, the relationship between the chloride diffusion coefficient and porosity of cement mortars is established by using the generalized effective medium theory [42, 43], as follows:

$$D_{cm} = \frac{2\varphi^{2.75} D_0}{\varphi^{1.75}(3-\varphi) + 14.44(1-\varphi)^{2.75}} \tag{11}$$

where D_{cm} is the chloride diffusion coefficient in cement mortars, and D_0 is the chloride diffusion coefficient in pore solution (1.07×10^{-10} m^2/s).

2.2.2 Chloride binding

The transport process of chloride ions satisfies the mass conservation, and it can be expressed by Eq. (12).

$$\frac{\partial C}{\partial t} = -\nabla J \tag{12}$$

where J is the ionic diffusion flux.

Since a part of chloride ions will be bound by hydration products, the chloride binding effect should also be considered. At this time, Eq. (12) needs to be further described as:

$$\frac{\partial(\varphi \cdot C_f)}{\partial t} + \frac{\partial((1-\varphi)C_b)}{\partial t} = -\varphi \cdot \nabla J \tag{13}$$

where C_f and C_b represent the free and bound chloride concentrations, respectively.

The concentrations of free and bound chloride ions in concrete are in a dynamic equilibrium. Thus, the bound chloride concentration can be expressed by Eq. (14), as follows:

$$\frac{\partial C_b}{\partial t} = -k_b\left(C_b - C_b^{eq}\right) \tag{14}$$

where k_b is the reaction rate constant for chloride binding (3.13×10^{-7} m^3/mol/s), and C_b^{eq} is the bound chloride concentration when the free and bound chloride concentrations reach an equilibrium.

The isothermal adsorption curves are frequently used to correlate free and bound chloride concentrations [44]. Here, Langmuir isotherm is used in the modelling to characterize the chloride binding effect, and the expression of C_b^{eq} is as follows:

$$C_b^{eq} = \frac{\alpha \cdot C_f}{1 + \beta \cdot C_f} \tag{15}$$

where α and β are the binding coefficients, which are taken as 0.42 and 0.8 L/mol, respectively [45].

It should be noted that concrete is a kind of heterogeneous material, and its local properties may vary at different areas. In the presented model, it is assumed that the local w/c and porosity do not change with location, that is, the chloride diffusivity and binding effect are considered to be the same everywhere in the cement mortar matrix.

2.2.3 *Electrochemical coupling between multi-species*

Apart from chloride ions, the pore solution in concrete also involves other ionic species, such as calcium [48], sodium, potassium, hydroxide, sulphate, etc. [46, 47, 49]. While ionic transport is commonly determined by Fick's law, it only considers the diffusion of a single ion at the macro scale, and it is difficult to accurately reflect the activity process of multiple species in concrete at the meso/micro scale [50]. Due to the differences in the charge properties and diffusion rates of various ions, it will generate charge imbalance between multi-species and create an electrostatic potential in local area of the concrete, which may affect the transportation of every ionic species [51–53]. Therefore, the influence of electrostatic potential between multi-species on the chloride transport process needs to be properly considered besides the concentration gradient.

Nernst-Planck equation can express the transportation process of an ionic species in the multi-component pore solution of concrete, as shown in Eq. (16).

$$J_k = -D_k \nabla C_k - \frac{z_k F}{RT} D_k C_k \nabla \Phi \tag{16}$$

where J_k, D_k, C_k and z_k are the ionic flux, diffusion coefficient, ionic concentration and charge number of the k-th ion, respectively, F is the Faraday constant (96,485 C/mol), R is the ideal gas constant (8.314 J/(mol·K)), T is the absolute temperature (298 K), and Φ is the electrostatic potential.

In the existing studies, researchers usually utilise the assumption of electro-neutrality to characterize the effect of ionic interaction. However, the electro-neutrality condition is more suitable for one-dimensional and single-phase models while does not accord with the real electrochemical law in multi-dimensional and multi-phase models, which will lead to the deviation of prediction results [54, 55]. In order to truly reflect the electrostatic potential at any point, Poisson's equation is used in the model to consider the electrochemical coupling effect between multiple ions (see Eq. 17).

$$\nabla^2 \Phi = -\frac{F}{\varepsilon_0 \varepsilon_r} \sum_{k=1}^{N} z_k C_k \tag{17}$$

where ε_0 is the permittivity of vacuum (8.85×10^{-12} F/m), ε_r is the relative permittivity of water at the temperature of 298 K (78.3), and N is the total number of all ionic species.

3 Modelling

3.1 Model establishment

In this study, a 3-D, three-phase fresh concrete model is established. The prismatic concrete specimen is in the size of 150 mm × 150 mm × 500 mm, including CAs, mortars and ITZs. The CA particle size is 5–20 mm, which is randomly generated based on the Fuller grading curve, and the CA volume fraction is 45%. The particle size distribution of CAs is shown in Appendix 2. Furthermore, the ITZ thickness between CAs and cement mortars is usually 20–50 μm in concrete according to previous findings [56, 57], and it is set as 40 μm in the presented model. It should be noted that the CA grading curve, CA volume fraction and ITZ thickness are assumed to be constant in this model. Of course, these parameters can be changed according to different needs.

Note that the settlement rate of large-sized CAs is faster than that of small-sized ones according to Eq. (4), which is easy to lead to the intersection of CAs with different particle sizes in the model. In order to solve this problem, the entire vibration process during modelling is superposed by many short-time steps with a vibration duration of 0.05 s, as presented in Fig. 2. At the end of each step, if it is determined that the CAs have intersected, the involved CAs particles

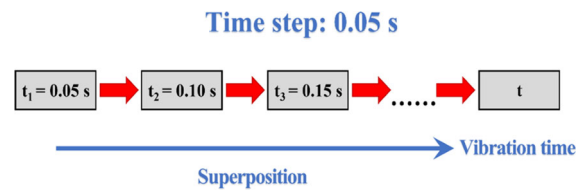

Fig. 2 Algorithm flow chart of the CA settlement model

are randomly bounced to the nearby empty space and the minimum spacing from each other is set as 100 μm. Likewise, the CAs in the bottom layer cannot intersect with the model boundary after settlement, and the minimum spacing between them is also set as 100 μm.

Figure 3 depicts the variation of CA distribution with vibration time in the 3-D settlement model. For easier direct observation of the CA settlement process, a 2-D section is extracted vertically from the middle of the 3-D model (see Fig. 3). It can be observed that with the progress of vibration, the CA content in the top part of concrete decreases obviously. For example, there are most of mortars and only few of CAs with a small particle size in the top layer area when the vibration duration reaches 25 s. Conversely, the distribution profile shows an increased CA content towards a lower height position of the concrete specimen because CAs gradually deposit to the bottom layer under the action of gravity. Regarding the CAs with different particle sizes, the large-sized CAs indeed perform a more significant settlement distance than the small-sized ones.

The concrete specimen is simulated to be immersed in a marine environment with a sodium chloride concentration of 886 mol/m^3, which is approximately equal to a 5 wt% sodium chloride solution. One side surface of the specimen is treated as an exposed surface, and other surfaces are set to be non-flux to ensure the one-dimensional transport of chloride ions in concrete. Note that the solution of ionic transport process in such a large-sized 3-D model is quite time-consuming, and sometimes it even fails to converge due to the high nonlinearity caused by internal ionic charge imbalance and electrostatic potential distribution. Considering that in most experiments, only one surface of the concrete specimen is immersed in sodium chloride solution, while the other surfaces are sealed with epoxy resin or paraffin wax, so the dominant transport direction is from the exposed surface to the interior, which is exactly represented by the 2-D model. Herein, five 2-D sections are extracted from each studied 3-D settlement model along the vertical direction for the modelling of ionic transport, and each corresponding result analysed and discussed in the following sections is determined by the average of them.

Taking a 2-D section of the CA settlement model with a vibration time of 25 s as an example, the finite element meshing of the model is depicted in Fig. 4, which displays that only the mortars and ITZs are meshed due to the impermeability of CAs. Note that in order to solve the problem of the tiny scale of ITZs, it is necessary to finely mesh the element size to obtain the convergent solutions. At the same time, a denser mesh will spend much more time on computation, although it can bring more accurate results. In this model, the minimum element size is 62.5 μm.

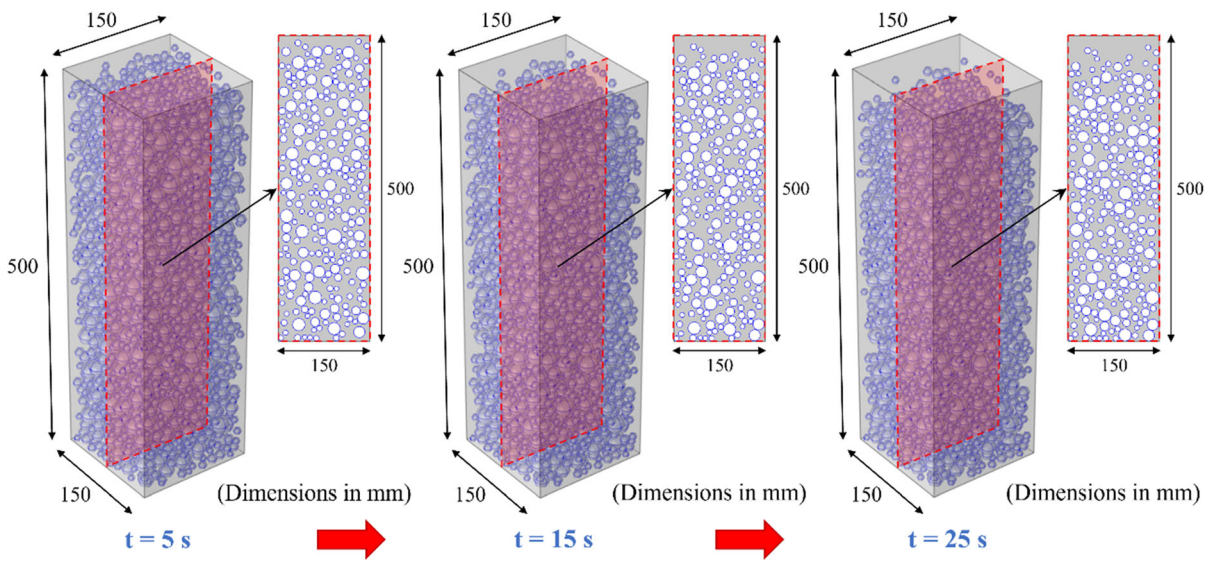

Fig. 3 Visualization display of CA settlement induced by vibration (adapted from [31])

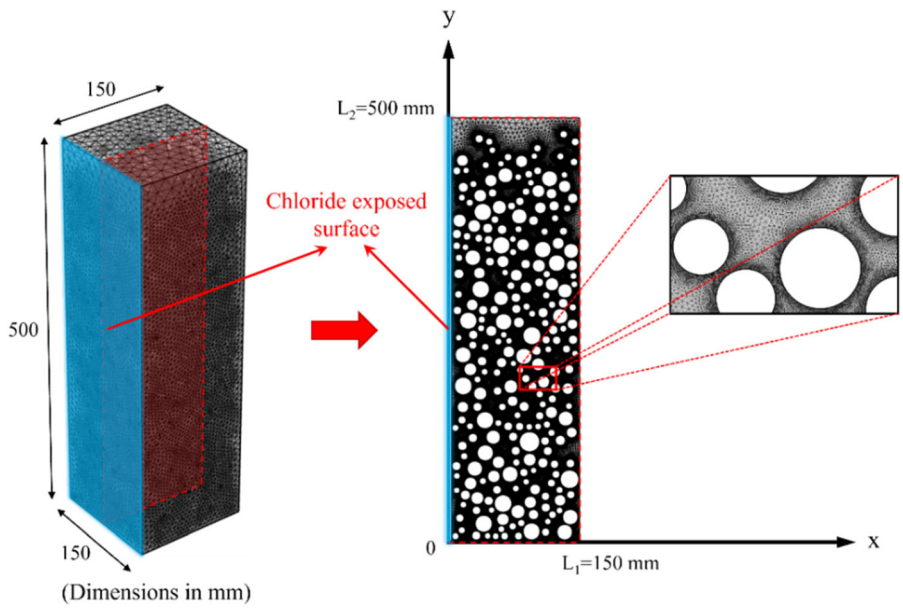

Fig. 4 An example of finite element meshing of a section of the CA settlement model (t = 25 s)

It should also be noted that concrete pore solution is an environment with multiple ionic species. In this study, only sodium, potassium, chloride and hydroxide ions are analysed to characterize the electrochemical coupling effect between them, since the concentrations of other ionic species like calcium and sulphate are rather low in the pore solution of concrete [58]. Table 1 provides the parameter information of these ionic species used in the current model. In addition, ITZ is a porous area with a higher permeability, where ionic species diffuse more easily. Considering that the current model is established at the mesoscopic scale, finite element meshing and calculation will be more difficult if the ITZ porosity variation is taken into account at a smaller scale. Here, the permeability of ITZs is considered to be average. Existing studies show that the ionic diffusion coefficient in ITZs (D_{itz}) is about 2−10 times that in mortars [59, 60]. In this study, D_{itz} is set as 5 times the ionic diffusion coefficient in mortars.

3.2 Model validation

Generally, the influence of CAs on ionic transport in concrete mainly includes the tortuosity effect, the dilution effect and the ITZ effect. The tortuosity effect refers to the fact that the presence of CAs may extend the transport path of ionic species. The dilution effect occurs because CAs are assumed to be impermeable, and aggressive species can only penetrate in the mortars and ITZs. The ITZ effect means that the ITZ on the surface of CAs is an area with a relatively high

Table 1 The parameter information of various ionic species used in the model

Ionic species	Charge number	Diffusion coefficient in the pore solution (m^2/s)	Initial concentration (mol/m^3)	Boundary concentration, x = 0	Boundary concentration, x = L_1
Sodium	1	0.66×10^{-10}	190	886 mol/m^3	0
Potassium	1	0.98×10^{-10}	380	0	0
Chloride	–1	1.07×10^{-10}	0	886 mol/m^3	0
Hydroxide	–1	1.63×10^{-10}	570	0	0

porosity compared to the surrounding cement mortars, which will promote the ingress of harmful ions into concrete. Therefore, the tortuosity effect and the dilution effect can improve the resistance of concrete to chloride ingress, whereas the ITZ effect is just the opposite [61–63].

Vibration-induced settlement can easily lead to the variability of CA volume fraction along the casting direction, and then affect the resistance to chloride penetration at different heights after concrete hardening. Since various settlement models with different parameter information have been well verified by experiments in previous study [31], this section mainly aims to validate whether the modelling results regarding the variation in chloride permeability along the height direction can be consistent with the existing experimental data. At present, only limited studies have been reported on the topic of the influence of CA settlement on the chloride transport properties of hardened concrete. Here, the experimental data of Gao et al. [10] and Cai et al. [12] are used to validate the applicability and reliability of the current model. Note that two different experimental methods, RCPT (refer to ASTM C1202–19 [64]) and NSSM (refer to NT Build 492 [65]), respectively, were in these two studies to test the chloride permeability of concrete specimen at different heights. To evaluate the heterogeneity of transport property along the height direction of concrete, the experimental results of charge passed and chloride migration coefficient at the top and bottom heights obtained based on these two methods are used to calculate the difference ratio of chloride permeability, as shown in Eq. (18).

$$S = 2 \times \frac{P_t - P_b}{P_t + P_b} \times 100\% \tag{18}$$

where S represents the difference ratio of chloride permeability along the height direction, and P_t and P_b represent the chloride permeability (charge passed, chloride migration coefficient or apparent chloride diffusion coefficient) of concrete specimen at the top and bottom heights, respectively.

The experimental data of chloride permeability of concrete at different heights and vibration durations are shown in Table 2. As can be seen from Table 2, the concrete at the bottom height of the specimen always shows a better chloride permeability resistance (lower charge passed or chloride migration coefficient) than that at the top height, and the difference ratio of chloride permeability between them becomes larger with the increase of vibration duration. This is because, under the action of vibration, CAs gradually settle to the bottom layer of concrete specimen. Although the increase of CA content in the bottom part of concrete will produce a larger area of ITZs with a high permeability, the tortuosity effect and dilution effect play a more crucial role in this study compared to ITZ effect, resulting in the reduction of chloride diffusion and transport performance.

At the same time, a series of CA settlement and ionic transport models have been developed, and the details of these models, such as the size of concrete specimen, vibration duration, etc., are set to be consistent with the experiments [10, 12]. Figure 5 displays the chloride concentration in concrete as a function of the penetration depth from the exposure surface. According to the test protocol of ASTM C1556-11a [66], the apparent chloride diffusion coefficients (D_a) are calculated by fitting Eq. (19) to the chloride profiles. As shown in Fig. 5, the concrete at the top height of the specimen always shows a larger apparent chloride diffusion coefficient than that at the bottom height. Furthermore, due to the occurrence of CA settlement, the apparent chloride diffusion coefficient of concrete at the top height and bottom height increases and decreases with vibration time, respectively.

$$C(x,t) = C_s - (C_s - C_i) \cdot erf\left(\frac{x}{\sqrt{4 \cdot D_a \cdot t}}\right) \tag{19}$$

where $C(x,t)$ is the chloride concentration tested at penetration depth x and exposure time t, C_s is the chloride concentration at the exposure surface, and C_i is the initial chloride concentration of the concrete before immersion in the sodium chloride solution.

Similarly, the modelling results of apparent chloride diffusion coefficient of concrete at different heights and vibration durations are listed in Table 2, and then the difference ratio of chloride permeability is also calculated by Eq. (18) for comparison with the experimental data. It can be seen from Fig. 6 that the prediction results of the difference rate of chloride permeability show a good correlation with the experimental data. Both modelling and experimental results can accurately and synchronously reflect the development law of the heterogeneous chloride penetration resistance along the height direction of concrete

Table 2 The experimental and modelling results of chloride permeability of concrete at different heights and vibration durations

Height (mm)	Details	Experiment				Model	
		Charge passed	Chloride migration coefficient	S (%)	Refs	D_a (m^2/s)	S (%)
50	Specimen size is 150 mm × 150 mm × 366 mm, and vibration duration is 15 s	2181 C	–	30.24	Gao et al. [10]	3.77×10^{-12}	27.66
316		2958 C	–			4.98×10^{-12}	
50	Specimen size is 150 mm × 150 mm × 366 mm, and vibration duration is 30 s	2215 C		61.48		3.46×10^{-12}	52.61
316		4181 C	–			5.93×10^{-12}	
150	Specimen size is 200 mm × 150 mm × 912 mm, and vibration duration is 25 s	–	3.33×10^{-12} m^2/s	39.90	Cai et al. [12]	3.61×10^{-12}	41.84
750		–	4.99×10^{-12} m^2/s			5.52×10^{-12}	

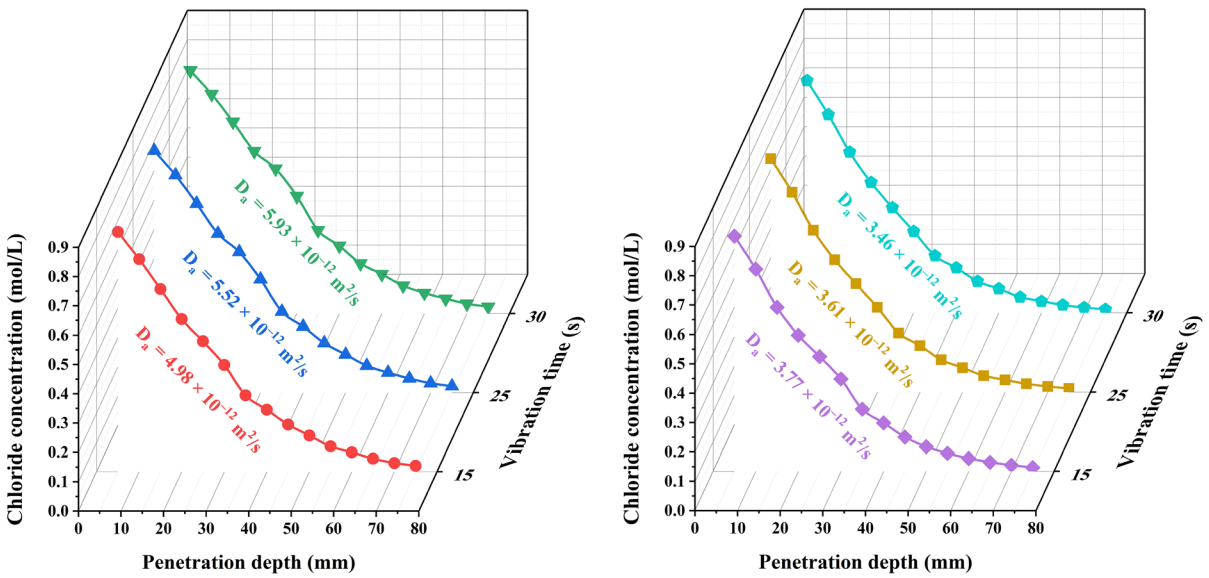

(a) Top height **(b)** Bottom height

Fig. 5 The fitting curves of chloride profiles used to determine D_a

specimen, that is, the concrete in the top part exhibits a higher chloride permeability than that in the bottom part, and the difference ratio of chloride permeability between them increases with vibration time. It demonstrates that the current model is applicable and reliable in this study.

4 Results and discussion

4.1 Effect of vibration time on chloride transport

In order to reveal the influence mechanism of vibration-induced CA settlement on the heterogeneity of

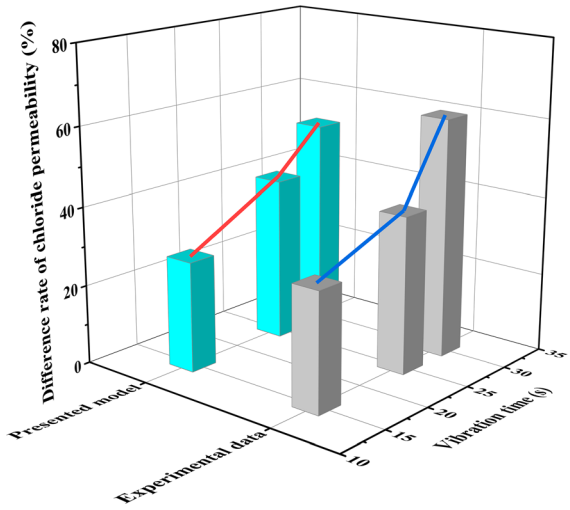

Fig. 6 Comparison of the difference rate of chloride permeability with vibration time between the model and experiment

long-term chloride penetration resistance of concrete, the testing ages were set as 5 years and 10 years, and the chloride profile distribution in the section from the middle of concrete specimen and perpendicular to the ionic transport direction was selected for discussion. At the chloride penetration depth of 75 mm, the influence of vibration time on the distribution of chloride concentration along the height direction of concrete specimen is shown in Fig. 7.

As displayed in Fig. 7, since CAs were randomly distributed in the internal space of concrete, the chloride concentration varied slightly along the casting direction before vibration even at the same penetration depth. Once the vibration started, the yield stress of concrete mixtures was significantly reduced or even ignored at vibrating state, and the CA particles settled downwards under the action of gravity. With the increase of vibration time, the CA content in the bottom part of concrete specimen increased gradually, and the chloride concentration in this area showed a decreasing trend after concrete hardening owing to the tortuosity effect and dilution effect. It was noteworthy that, when the vibration duration increased to a certain extent, due to the dense packing of some CA particles in the bottom layer, the variation degree of chloride concentration would gradually decrease with vibration time.

In addition, the CA content decreased with the increase of the height of concrete specimen, resulting in an obvious increase in the chloride concentration, especially in the top 50 mm height area. Taking the vibration time of 25 s as an example, the chloride concentrations at the height of 25 mm were 12.0 mol/m^3 and 68.1 mol/m^3 in the testing ages of 5 years and 10 years, respectively. When the height position was increased to 475 mm, the chloride concentrations at these two testing ages had reached 21.3 mol/m^3 and 97.7 mol/m^3, respectively, i.e., increased by 77.5% and 43.5%, respectively. This was in accordance with the visual analysis observed in Fig. 3. When the vibration duration was 25 s, there were most of cement

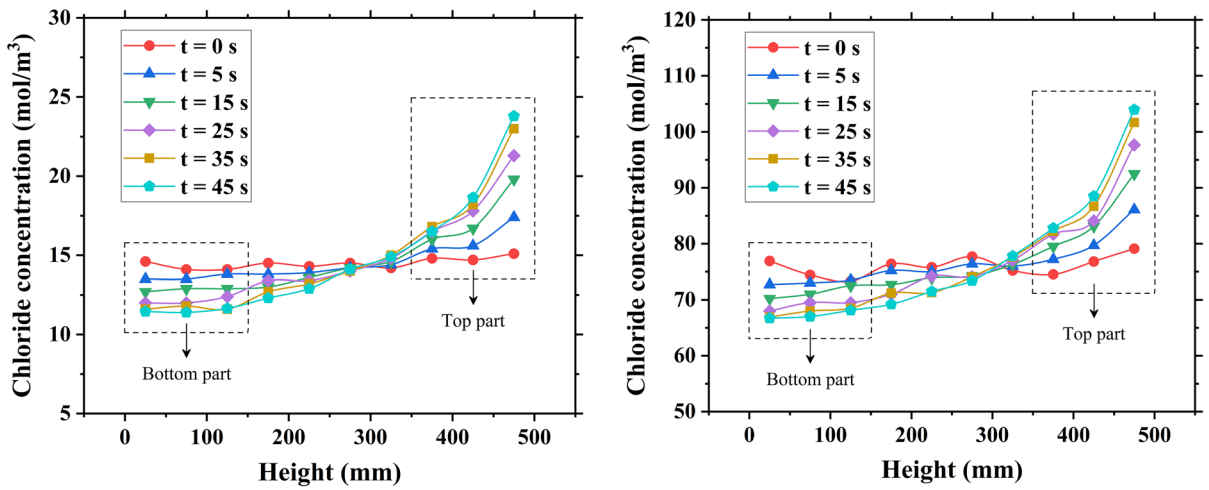

(a) 5 years **(b)** 10 years

Fig. 7 Effect of vibration time on chloride concentration distribution at 75 mm depth

mortars and only a few of small-sized CAs in the top part of concrete, which weakened the resistance capability to chloride penetration in this area. It should be noted that excessive vibration duration should be avoided in engineering practice since it can aggravate the degree of CA settlement, and the non-uniformity of CA distribution may lead to the earlier deterioration of long-term performance in the top part of hardened concrete due to the chloride contamination with a high concentration in this area.

4.2 Effect of CA density on chloride transport

In addition to vibration time, the properties of CAs such as density, particle size, volume fraction and grading might also change the degree of the influence of vibration-induced settlement on long-term chloride transport in concrete. Figure 8 shows the effect of CAs with different densities of 2.52 g/cm^3, 2.67 g/cm^3 and 2.79 g/cm^3 on chloride profile distribution when the vibration time was fixed at 25 s. It was worth noting that the reason for selecting CAs with these three densities was that the corresponding settlement models had been well verified by experiments [31], while the case of CAs with other densities was not discussed here.

As presented in Fig. 8, a more obvious fluctuation of chloride concentration along the height direction can be observed in the concrete mixed with a larger density of CAs. This variation is reflected in a higher content of chloride ions in the top part of concrete specimen and a lower content in the bottom part. When the height position increased from 25 to 475 mm, the increase rates of chloride concentrations in the testing ages of 5 years and 10 years were 58.3% and 33.1%, respectively, on the premise that the CA density was 2.52 g/cm^3. When the density of CAs increased to 2.79 g/cm^3, the increase rates of chloride concentrations in these two testing ages could reach 97.4% and 50.1%, respectively. This was because the density of CA particles used in this study was greater than that of mortar matrix, and a larger density difference between them would occur when the concrete mixtures mixed with a larger density of CAs, thereby leading to a greater settlement tendency. This was consistent with the experimental results obtained by Navarrete and Lopez [27, 67], who found that for a given concrete mixture, the settlement rate increased linearly with the density difference between CA particles and cement mortars.

4.3 Effect of CA particle size on chloride transport

In Fig. 9, the settlement models with CA particle sizes of 5–16 mm, 5–20 mm and 9.5–20 mm verified by experiments [31] were developed to study the effect of particle size of CAs on chloride transport in concrete. It was found that for a certain CA volume fraction and vibration time, the variation degree of chloride concentration along the height direction was more

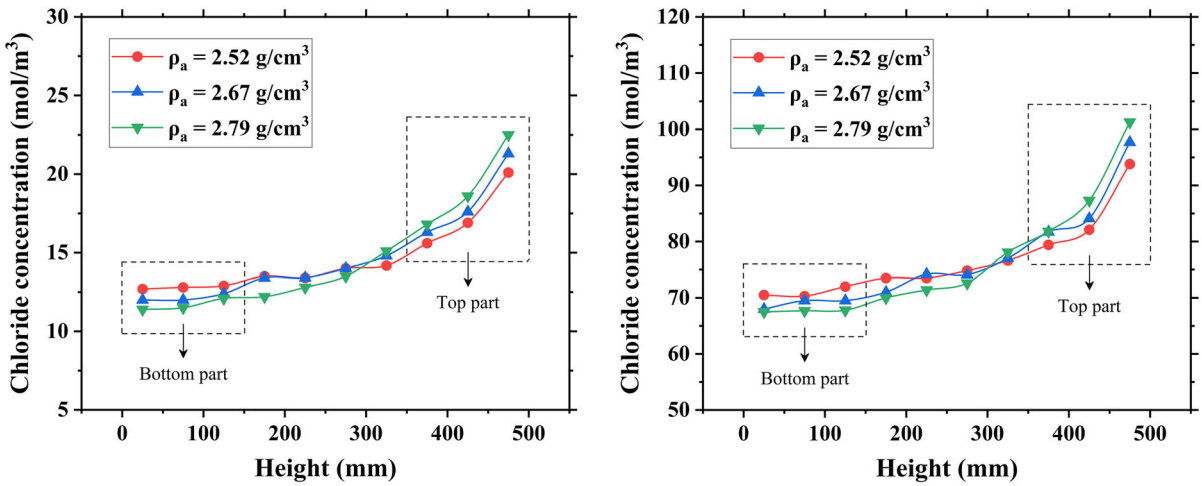

Fig. 8 Effect of CA density on chloride concentration distribution at 75 mm depth

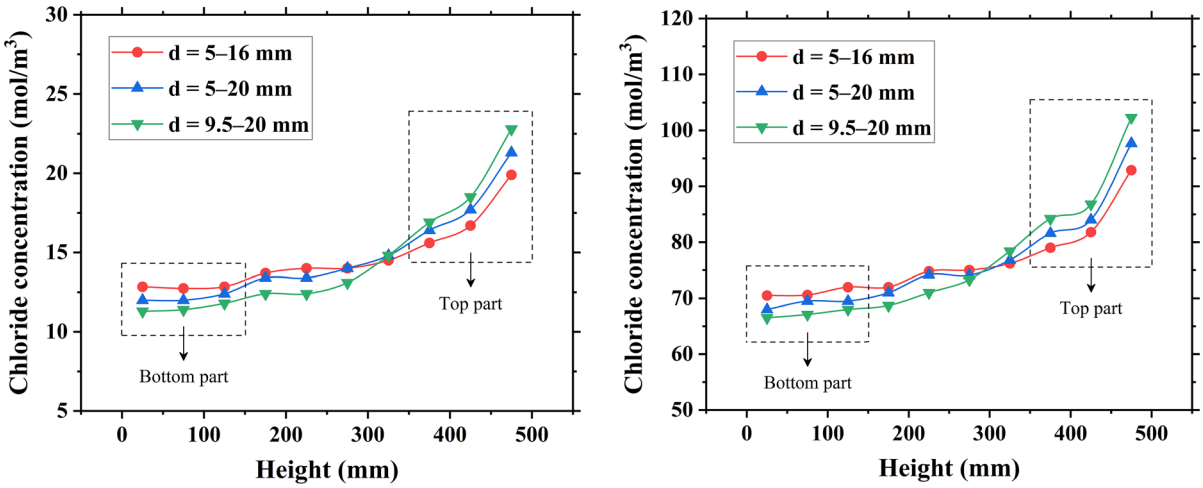

Fig. 9 Effect of CA particle size on chloride concentration distribution at 75 mm depth

obvious in the concrete mixed with more large-sized CAs. When the particle size distribution of CAs was 5–16 mm, the increase rates of chloride concentrations in the testing ages of 5 years and 10 years were 54.2% and 31.8%, respectively, as the height position increased from 25 to 475 mm. Nevertheless, when the particle size distribution of CAs changed to 9.5–20 mm, the increase rates of chloride concentrations in these two testing ages had reached 101.7% and 53.8%, respectively. This was because the settlement rate of the CA increased with its particle size, and the concrete mixtures containing more large-sized CA particles showed a greater settlement degree [68, 69].

4.4 Effect of ITZ diffusivity property on chloride transport

In concrete composites, the interface between CAs and mortar matrix is a porous and highly permeable area, and the impact of its diffusivity property on chloride transport should also be properly taken into consideration. Different ratios of the diffusion coefficients of ITZs to cement mortars (D_{itz}/D_{cm}) such as 3, 5, 7 and 9 with the same ITZ thickness were developed to understand the effect of diffusivity property of ITZs on long-term chloride transport in concrete. The chloride profile distribution along the height direction of concrete specimen is presented in Fig. 10. With the increase of D_{itz}/D_{cm}, the chloride concentration at the same height increased evidently owing to the contribution of a larger diffusion coefficient at the position of ITZ area.

Moreover, the settlement induced by vibration made more CAs deposit to the bottom layer of concrete, and the tortuosity effect and dilution effect limited the chloride ingress at a low height position. It should be noted that there was a more obvious difference in chloride concentration between various groups with different D_{itz}/D_{cm} in the bottom layer, but this difference was significantly lower in the top layer of the concrete specimen due to the steep reduction in CA content. These results demonstrated that a lower ITZ diffusivity helped to limit chloride ingress into the concrete, especially in the bottom area of specimen. Therefore, the performance optimization of the interface between CAs and mortars is an important way to ensure longer service life of structural concrete, which needs more attention in the future.

4.5 Prediction of reinforcement corrosion initiation

In the marine environment or as a consequence of using de-icing salt, chloride ions penetrate into the surface of embedded steel bars through the concrete cover. Once the chloride content around the steel bars reaches a threshold level, reinforcement corrosion begins, leading to serious damage to the reinforced concrete structures [21–25]. Hence, it is possible to use the numerical model to predict the long-term

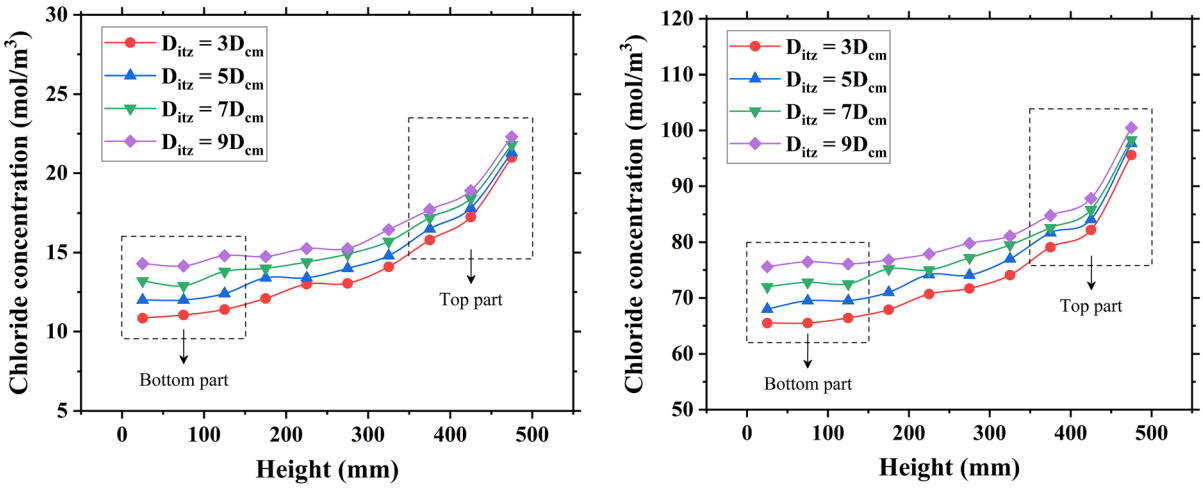

Fig. 10 Effect of ITZ diffusivity property on chloride concentration distribution at 75 mm depth

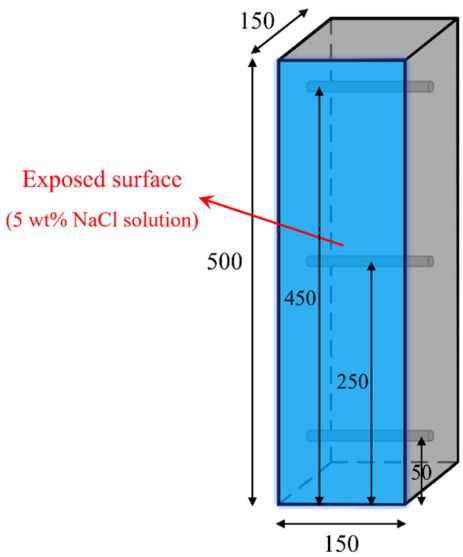

Fig. 11 Layout of the reinforced concrete specimen (unit: mm)

chloride transport and its effect on the reinforcement corrosion onset in concrete. The reinforced concrete specimen is simulated to be immersed in a 5 wt% sodium chloride solution, and three steel bars are assumed to be cast horizontally in the top, middle and bottom heights (450 mm, 250 mm and 50 mm), respectively, as show in Fig. 11. Here, only one side (blue surface) is treated as the exposed surface, and the steel bars are arranged in the middle of specimen and perpendicular to the direction of chloride transportation. It means the chloride concentration at the penetration depth of 75 mm can be approximately regarded as the chloride content near the surface of steel bars.

Figure 12 depicts the development of chloride concentration at the surface of steel bars with immersion time under different parameters. As observed, at the same testing age, the chloride concentration at the surface of the top steel bar was always higher than that at the surfaces of the middle and bottom steel bars. From the result, it could be considered that the reinforcing steel arranged in the top part of specimen tended to corrode earlier. In order to quantitatively describe the effect of CA settlement on the corrosion initiation time of steel bars, the critical chloride level of reinforcement corrosion (C_{crit}) was assumed to be 55 mol/m^3. Note that it might not in any way represent the real conditions where the critical chloride level might change due to a number of factors, and the value of 55 mol/m^3 was only used for demonstration purposes.

The prediction results of time for reinforcement corrosion onset in concrete are summarized in Table 3. As for the parameter of vibration time, Table 3 only shows the prediction results of vibrating durations of 15 s, 25 s and 35 s, since it is usually 15–35 s in practical applications. It can be found that in all groups of different parameters, the corrosion of the top steel bar initiates 1.03–1.80 years earlier than that of the

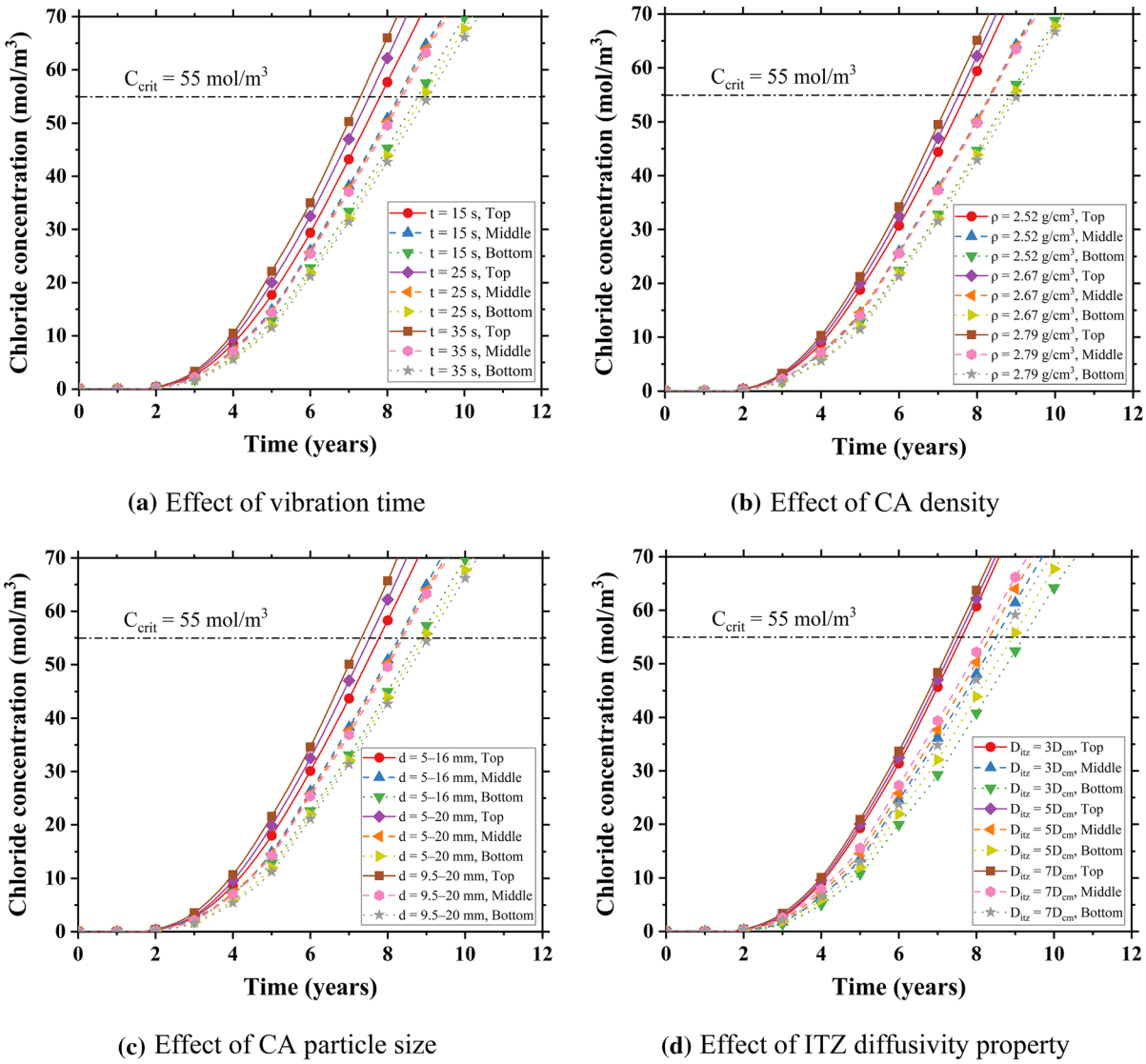

(a) Effect of vibration time

(b) Effect of CA density

(c) Effect of CA particle size

(d) Effect of ITZ diffusivity property

Fig. 12 Long-term development of chloride concentration at the surface of steel bars

bottom steel bar. As mentioned above, chloride ions penetrate into concrete faster at a higher position due to CA settlement, which is one of the key reasons for the earlier corrosion initiation of top rebars. Additionally, there is also an effect that is not considered in the model: the top steel bar tends to have more air voids underneath due to segregation and micro-bleeding, and these air voids tend to be initiation sites for corrosion. This may also accelerate the corrosion process, and further exacerbate the difference in corrosion initiation time between top and bottom steel bars [70–73].

Discriminating between the effect of CA settlement and long-term durability of the top part of concrete specimens in comparison to the bottom part is of particular importance in context with real world applications. For cast-in-place structures, the top surface is commonly exposed to the environment composed of ionic species and moisture, and vibration-induced settlement leads to the easier invasion of harmful substances from outer environment into concrete. Nowadays, much attention is paid on the mix proportion, binder composition and use of admixtures to improve the durability of reinforced

Table 3 Prediction of time for reinforcement corrosion onset

Group	Parameters				Initiation time of reinforcement corrosion (years)		
	Vibration time (s)	CA density (g/cm^3)	CA particle size (mm)	ITZ diffusivity property (D_{itz}/D_{cm})	Top	Middle	Bottom
1	15	2.67	5–20	5	7.79	8.30	8.82
2	25	2.67	5–20	5	7.50	8.36	8.96
3	35	2.67	5–20	5	7.27	8.41	9.07
4	25	2.52	5–20	5	7.68	8.35	8.87
5	25	2.79	5–20	5	7.33	8.39	9.04
6	25	2.67	5–16	5	7.76	8.31	8.83
7	25	2.67	9.5–20	5	7.29	8.40	9.06
8	25	2.67	5–20	3	7.59	8.52	9.23
9	25	2.67	5–20	7	7.42	8.21	8.67

concrete. Apart from these, fresh concrete stability and vibrating procedures should also be given special attention in practical engineering to prevent obvious CA settlement induced by vibration. In addition, the current work mainly focuses on normal concrete system. With the increasing use of self-compacting concrete in constructions, the impact of its stability on long-term durability performance should also be concerned. But it is noteworthy that the rheological behaviour of fresh concrete with or without need of vibration is quite different, the mechanism research on this topic is worth exploring in future work.

5 Conclusions

In this paper, a numerical study combining CA settlement model and ionic transport model is performed to reveal the influence mechanism of vibration-induced settlement on long-term chloride transport in concrete. The following conclusions can be drawn:

1. Although the occurrence of CA settlement will produce a larger area of ITZs with a high permeability in the bottom part of concrete, the tortuosity effect and dilution effect play a more crucial role compared to ITZ effect in this study. As the vibration time increases, the chloride concentration in the bottom part shows a decreasing trend due to the deposition of more CAs in this area.
2. CA content decreases with the increase of the height position of concrete, resulting in an obvious increase in the chloride concentration, especially in the top 50 mm height area of the specimen. Taking the vibration time of 25 s as an example, the chloride concentrations in the testing ages of 5 years and 10 years increase by 77.5% and 43.5%, respectively, when the height increases from 25 to 475 mm.
3. Due to the settlement caused by vibration, a more obvious fluctuation of chloride concentration along the height direction can be observed in the concrete mixed with a larger density and particle size of CAs. A lower ITZ diffusivity property helps to limit chloride ingress into the concrete, especially in the bottom area of specimen.
4. Since vibration-induced settlement results in a remarkable reduction in CA content in the top layer, it weakens the resistance to chloride penetration in this area. The model prediction results of reinforcement corrosion initiation demonstrate that the corrosion of the top steel bar initiates 1.03–1.80 years earlier than that of the bottom steel bar under the same parameters.

Acknowledgements This work was funded by the National Natural Science Foundation of China (51978396, 52222805), the Natural Science Foundation of Shanghai, China (22ZR1431400), and the Oceanic Interdisciplinary Program of Shanghai Jiao Tong University, China (SL2021MS016).

Declarations

Conflict of interest The authors declare that they have no conflict of interest.

Appendix 1

The acceleration of CA movement (a) is expressed as:

$$a = \frac{g(\rho_a - \rho_m)}{\rho_a} - \frac{18\eta_{pl}}{d^2\rho_a} \cdot v \tag{20}$$

Assumptions:

$$M = \frac{g(\rho_a - \rho_m)}{\rho_a} \tag{21}$$

$$N = \frac{18\eta_{pl}}{d^2\rho_a} \tag{22}$$

Equation (20) can be further expressed as:

$$\frac{\mathrm{d}v}{\mathrm{d}t} = M - N \cdot v \tag{23}$$

The expression of v can be obtained by solving Eq. (23):

$$v = \frac{M}{N} - \frac{M}{N} \cdot \exp(-N \cdot t) \tag{24}$$

Through integral calculation, the CA settlement height is expressed as:

$$\Delta h = \frac{M}{N} \cdot t - \frac{M}{N^2} + \frac{M}{N^2} \cdot \exp(-N \cdot t) \tag{25}$$

Bring Eqs. (21) and (22) into Eq. (25), that is:

$$\Delta h = \frac{d^2 g(\rho_a - \rho_m)}{18\eta_{pl}} \cdot \left\{ t - \frac{d^2\rho_a}{18\eta_{pl}} \cdot \left[1 - \exp\left(-\frac{18\eta_{pl}}{d^2\rho_a} \cdot t \right) \right] \right\} \tag{26}$$

Appendix 2

See Fig. 13.

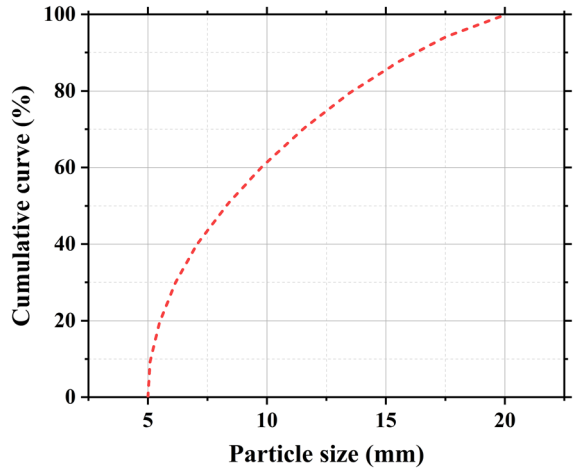

Fig. 13 Particle size distribution of CAs

References

1. Aïssoun BM, Hwang SD, Khayat KH (2016) Influence of aggregate characteristics on workability of superworkable concrete. Mater Struct 49:597–609
2. Jang KP, Kwon SH, Choi MS, Kim YJ, Park CK, Shah SP (2018) Experimental observation on variation of rheological properties during concrete pumping. Int J Concr Struct Mater 12:79
3. Koch JA, Castaneda DI, Ewoldt RH, Lange DA (2019) Vibration of fresh concrete understood through the paradigm of granular physics. Cem Concr Res 115:31–42
4. Safayenikoo H, Khajehzadeh M, Nehdi ML (2022) Novel evolutionary-optimized neural network for predicting fresh concrete slump. Sustainability 14(9):4934
5. Roussel N (2006) A theoretical frame to study stability of fresh concrete. Mater Struct 39(1):81–91
6. Pan J, He J, Zhu J, Gao X (2022) Theoretical and experimental study on the electrical resistivity method for evaluating fresh concrete segregation. J Build Eng 48:103943
7. Muslim F, Wong HS, Cheng G, Alexandrou C, Liu B, Buenfeld NR (2020) Combined effects of vertical spacers and segregation on mass transport properties of reinforced concrete. Mater Struct 53:151
8. Khayat KH, Manai K, Trudel A (1997) In situ mechanical properties of wall elements cast using self-consolidating concrete. ACI Mater J 94(6):491–500
9. Megid WA, Khayat KH (2018) Effect of concrete rheological properties on quality of formed surfaces cast with self-consolidating concrete and superworkable concrete. Cem Concr Compos 93:75–84
10. Gao X, Zhang J, Su Y (2019) Influence of vibration-induced segregation on mechanical property and chloride ion permeability of concrete with variable rheological performance. Constr Build Mater 194:32–41

11. Panesar DK, Shindman B (2012) The effect of segregation on transport and durability properties of self consolidating concrete. Cem Concr Res 42:252–264
12. Cai Y, Zhang W, Yu L, Chen M, Yang C, François R, Yang K (2020) Characteristics of the steel-concrete interface and their effect on the corrosion of steel bars in concrete. Constr Build Mater 253:119162
13. Cai Y, Zhang W, Yang C, François R, Yu L, Chen M, Chen H, Yang H (2021) Evaluating the chloride permeability of steel–concrete interface based on concretes of different stability. Struct Concr 22(5):2636–2649
14. Zhang W, François R, Wang R, Cai Y, Yu L (2020) Corrosion behavior of stirrups in corroded concrete beams exposed to chloride environment under sustained loading. Constr Build Mater 274:121987
15. Liu QF, Iqbal MF, Yang J, Lu XY, Zhang P, Rauf M (2021) Prediction of chloride diffusivity in concrete using artificial neural network: modelling and performance evaluation. Constr Build Mater 268:121082
16. Ashraf M, Iqbal MF, Rauf M, Ashraf MU, Ulhaq A, Liu QF (2022) Developing a sustainable concrete incorporating bentonite clay and silica fume: mechanical and durability performance. J Cleaner Prod 337:130315
17. Chen M, Wei Y, Zheng H, Yu L, Liu Q, Wang Y, Yuan H, Wang C, Li W (2022) Ca-LDH-modified cementitious coating to enhance corrosion resistance of steel bars. J Build Eng 51:104301
18. Liu QF, Hu Z, Wang XE, Zhao H, Qian K, Li LJ, Meng Z (2022) Numerical study on cracking and its effect on chloride transport in concrete subjected to external load. Constr Build Mater 325:126797
19. Li LJ, Liu QF (2022) Freezing rate and chloride transport in concrete subjected to freeze-thaw cycles: a numerical study. J Chin Ceram Soc 50(8):2245–2256
20. Tong L, Liu QF (2023) Multi-scale prediction model of chloride diffusivity of fiber reinforced concrete. Acta Mater Compositae Sin 40:1–12 https://doi.org/10.13801/j.cnki.fhclxb.20220422.003
21. Angst U, Elsener B, Larsen CK, Vennesland Ø (2009) Critical chloride content in reinforced concrete—a review. Cem Concr Res 39(12):1122–1138
22. Mundra S, Criado M, Bernal SA, Provis JL (2017) Chloride-induced corrosion of steel rebars in simulated pore solutions of alkali-activated concretes. Cem Concr Res 100:385–397
23. Zhang W, François R, Cai Y, Charron JP, Yu L (2020) Influence of artificial cracks and interfacial defects on the corrosion behavior of steel in concrete during corrosion initiation under a chloride environment. Constr Build Mater 253:119165
24. Meng Z, Liu QF, She W, Cai Y, Yang J, Iqbal MF (2021) Electrochemical deposition method for load-induced crack repair of reinforced concrete structures: a numerical study. Eng Struct 246:112903
25. Chen M, Cai Y, Zhang M, Yu L, Wu F, Jiang J, Yang H, Bi R, Yu Y (2021) Novel Ca-SLS-LDH nanocomposites obtained via lignosulfonate modification for corrosion protection of steel bars in simulated concrete pore solution. Appl Clay Sci 211:106195
26. Petrou MF, Harries KA, Gadala-Maria F, Kolli VG (2000) A unique experimental method for monitoring aggregate settlement in concrete. Cem Concr Res 30(5):809–816
27. Navarrete I, Lopez M (2017) Understanding the relationship between the segregation of concrete and coarse aggregate density and size. Constr Build Mater 149:741–748
28. Khayat KH, Pavate TV, Assaad J, Jolicoeur C (2003) Analysis of variations in electrical conductivity to assess stability of cement-based materials. ACI Mater J 100(4):302–310
29. Benaicha M, Jalbaud O, Roguiez X, Alaoui AH, Burtschell Y (2015) Prediction of self-compacting concrete homogeneity by ultrasonic velocity. Alex Eng J 54(4):1181–1191
30. Gokce HS, Ozturk BC, Çam NF, Andiç-Çakir O (2018) Gamma-ray attenuation coefficients and transmission thickness of high consistency heavyweight concrete containing mineral admixture. Cem Concr Compos 92:56–69
31. Cai Y, Liu QF, Yu L, Meng Z, Hu Z, Yuan Q, Savija B (2021) An experimental and numerical investigation of coarse aggregate settlement in fresh concrete under vibration. Cem Concr Compos 122:104153
32. Petrou MF, Wan BL, Gadala-Maria F, Kolli VG, Harries KA (2000) Influence of mortar rheology on aggregate settlement. ACI Mater J 97(4):479–485
33. Tattersall GH, Baker PH (1989) An investigation into the effect of vibration on the workability of fresh concrete using a vertical pipe apparatus. Mag Concr Res 41(146):3–9
34. Banfill PFG, Xu Y, Domone PLJ (1999) Relationship between the rheology of unvibrated fresh concrete and its flow under vibration in a vertical pipe apparatus. Mag Concr Res 51(3):181–190
35. Li Z, Cao G (2019) Rheological behaviors and model of fresh concrete in vibrated state. Cem Concr Res 120:217–226
36. Petit JY, Wirquin E, Vanhove Y, Khayat KH (2007) Yield stress and viscosity equations for mortars and self-consolidating concrete. Cem Concr Res 37(5):655–670
37. Leemann A, Winnefeld F (2007) The effect of viscosity modifying agents on mortar and concrete. Cem Concr Compos 29(5):341–349
38. Tong LY et al (2023) Modelling the chloride transport in concrete: from microstructure generation to chloride diffusivity prediction. Comput Struct
39. Hansen TC (1986) Physical structure of hardened cement paste: a classical approach. Mater Struct 19:423–436
40. Bentz DP, Garboczi EJ, Lagergren ES (1998) Multi-scale microstructural modelling of concrete diffusivity: identification of significant variables. Cem Concr Aggreg 20:129–139
41. Xiong QX et al (2023) A new analytical method to predict permeability properties of cementitious mortars: the impacts of pore structure evolutions and relative humidity variations. Cem Concr Compos
42. Zheng J, Zhou X (2008) Analytical solution for the chloride diffusivity of hardened cement paste. J Mater Civ Eng 20(5):384–391
43. Yu H, Da B, Ma H, Zhu H, Yu Q, Ye H, Jing X (2017) Durability of concrete structures in tropical atoll environment. Ocean Eng 135:1–10
44. Tang L, Nilsson LO (1993) Chloride binding capacity and binding isotherms of OPC pastes and mortars. Cem Concr Res 23(2):247–253
45. Li LJ, Liu QF, Tang L, Hu Z, Wen Y, Zhang P (2021) Chloride penetration in freeze–thaw induced cracking

concrete: a numerical study. Constr Build Mater 302:124291
46. Liu QF (2018) Multi-phase modelling of concrete at meso-micro scale based on multi-species transport. J Chin Ceram Soc 46(08):1074–1080
47. Chen WK, Liu QF (2021) Moisture and multi-ions transport in concrete under drying-wetting cycles: a numerical study. J Hydraul Eng 52(5):622–632
48. Liu QF, Shen XH, Šavija B, Meng Z, Tsang DCW, Sepasgozar S, Schlangen E (2023) Numerical study of interactive ingress of calcium leaching, chloride transport and multi-ions coupling in concrete. Cem Concr Res
49. Liu QF, Meng Z, Hou D, Zhou Y, Cai Y, Zhang M, Tam VWY (2022) Numerical modelling on electrochemical deposition technique for healing alkali silica reaction induced damaged concrete. Eng Fract Mech. https://doi.org/10.1016/j.engfracmech
50. Tong LY et al (2023) Modelling of chloride transport in concrete by considering the heterogeneous characteristics from micro- to macro-scale. Constr Build Mater
51. Elakneswaran Y, Iwasa A, Nawa T, Sato T, Kurumisawa K (2010) Ion-cement hydrate interactions govern multi-ionic transport model for cementitious materials. Cem Concr Res 40(12):1756–1765
52. Liu Y, Shi X (2012) Ionic transport in cementitious materials under an externally applied electric field: Finite element modelling. Constr Build Mater 27:450–460
53. Hu Z, Liu QF (2023) Numerical study of multi-species transport in cracked concrete under external load. Mater Rep 37(9):21120077
54. Johannesson B (2010) Comparison between the Gauss' law method and the zero current method to calculate multi-species ionic diffusion in saturated uncharged porous materials. Comput Geotech 37:667–677
55. Meng Z, Liu QF, Xia J, Cai Y, Zhu X, Zhou Y, Pel L (2022) Mechanical–transport–chemical modeling of electrochemical repair methods for corrosion-induced cracking in marine concrete. Comput Aided Civ Inf 37:1854–1874
56. Diamond S, Huang JD (2001) The ITZ in concrete—a different view based on image analysis and SEM observations. Cem Concr Compos 23(2–3):179–188
57. Liu QF, Feng GL, Xia J, Yang J, Li LY (2018) Ionic transport features in concrete composites containing various shaped aggregates: a numerical study. Compos Struct 183:371–380
58. Yu Y, Gao W, Feng Y, Castel A, Chen X, Liu A (2021) On the competitive antagonism effect in combined chloride-sulfate attack: a numerical exploration. Cem Concr Res 144:106406
59. Shane JD, Mason TO, Jennings HM, Garboczi EJ, Bentz DP (2000) Effect of the interfacial transition zone on the conductivity of portland cement mortars. J Am Ceram Soc 83(5):1137–1144
60. Wu L, Ju X, Liu M, Guan L, Ma Y, Li M (2020) Influences of multiple factors on the chloride diffusivity of the interfacial transition zone in concrete composites. Compos B Eng 199:108236
61. Abyaneh SD, Wong HS, Buenfeld NR (2013) Modelling the diffusivity of mortar and concrete using a three-dimensional mesostructure with several aggregate shapes. Comput Mater Sci 78:63–73
62. Gao Y, De Schutter G, Ye G, Tan Z, Wu K (2014) The ITZ microstructure, thickness and porosity in blended cementitious composite: effects of curing age, water to binder ratio and aggregate content. Compos B Eng 60:1–13
63. Niknezhad D, Raghavan B, Bernard F, Kamali-Bernard S (2015) Towards a realistic morphological model for the meso-scale mechanical and transport behavior of cementitious composites. Compos B Eng 81:72–83
64. ASTM C1202–19 (2019) Standard test method for electrical indication of Concrete's Ability to Resist Chloride Ion Penetration, Annual Book of ASTM Standards
65. NT Build 492 (1999) Concrete, mortar and cement-based repair materials: chloride migration coefficient from non-steady-state migration experiments, Nordtest Method.
66. ASTM C1556–11a (2011) Standard test method for determining the apparent chloride diffusion coefficient of cementitious mixtures by bulk diffusion, Annual Book of ASTM Standards
67. Navarrete I, Lopez M (2016) Estimating the segregation of concrete based on mixture design and vibratory energy. Constr Build Mater 122:384–390
68. Safawi MI, Iwaki I, Miura T (2004) The segregation tendency in the vibration of high fluidity concrete. Cem Concr Res 34(2):219–226
69. Shen L, Jovein HB, Wang Q (2016) Correlating aggregate properties and concrete rheology to dynamic segregation of self-consolidating concrete. J Mater Civ Eng 28(1):04015067
70. Angst UM, Geiker MR, Alonso MC, Polder R, Isgor OB, Elsener B, Wong H, Michel A, Hornbostel K, Gehlen C, François R, Sanchez M, Criado M, Sørensen H, Hansson C, Pillai R, Mundra S, Gulikers J, Raupach M, Pacheco J, Sagüés A (2019) The effect of the steel–concrete interface on chloride-induced corrosion initiation in concrete: a critical review by RILEM TC 262-SCI. Mater Struct 52:88
71. Rossi E, Polder R, Copuroglu O, Nijland T, Šavija B (2020) The influence of defects at the steel/concrete interface for chloride-induced pitting corrosion of naturally-deteriorated 20-years-old specimens studied through X-ray computed tomography. Constr Build Mater 235:117474
72. Rossi E, Zhang H, Garcia SJ, Bijleveld J, Nijland TG, Copuroglu O, Polder RB, Šavija B (2021) Analysis of naturally-generated corrosion products due to chlorides in 20-year old reinforced concrete: an elastic modulus-mineralogy characterization. Corros Sci 184:109356
73. Yu L, François R, Gagné R (2016) Influence of steel-concrete interface defects induced by top-casting on development of chloride-induced corrosion in RC beams under sustained loading. Mater Struct 49:5169–5181